Available online at www.sciencedirect.com
SCIENCE DIRECT
Applied Catalysis A: General 298 (2006) 232–242
APPLIED CATALYSIS A: GENERAL
www.elsevier.com/locate/apcata

Synthesis, characterization and selective oxidation properties of Ti-containing mesoporous catalysts

Griselda A. Eimer, Sandra G. Casuscelli, Guillermo E. Ghione, Mónica E. Crivello, Eduardo R. Herrero *

CITeQ (Centro de Investigación y Tecnología Química), Facultad Regional Córdoba, Universidad Tecnológica Nacional, CC36, Suc. 16 (5016) Córdoba, Argentina

Received 3 June 2005; received in revised form 22 September 2005; accepted 8 October 2005
Available online 17 November 2005

Abstract

Ti-containing mesoporous catalysts with MCM-41 structure have been successfully prepared by direct hydrothermal synthesis. These mesoporous materials were compared with pure siliceous MCM-41 synthesized at the same conditions. An extended and detailed study, which includes the effects of several factors such as the state and content of Ti, surfactant/Si ratio and template removal technique on the physicochemical properties and catalytic activity of Ti-MCM-41, is presented in this contribution. Various techniques including XRD, FT-IR, DRUV–vis, ICP and N_2 adsorption were employed for the materials characterization. An optimum surfactant/Si molar ratio in the synthesis gel for the highest regularity of the formed mesostructure was found. Both the structure stability and the local environment of Ti sites in mesostructures with different degrees of Ti loading (0.10–3.22 wt.%) have been carefully investigated. Based on a combined FT-IR and DRUV–vis study and ICP analysis, it was possible to conclude that Infrared spectroscopy can result a powerful tool to verify the Ti(IV) incorporation into the framework of MCM-41. Therefore, a simple and novel method for estimation of framework Ti content could be developed. Also, these materials were catalytically tested in the oxidation of cyclohexene with aqueous hydrogen peroxide. Finally, the catalysts could be regenerated without any loss in activity/selectivity.

Keywords: Ti-MCM-41; Mesoporous materials; M41S; Titanium; Epoxidation; Cyclohexene

1. Introduction

The new family of micelle-templated mesoporous molecular sieves with regular pore diameters (20–100 Å) and large surface areas (1000–1400 m^2/g), usually known as M41S, has aroused a great interest in the scientific community since the beginning of the 1990s [1–8]. Among the different ordered mesoporous structures, the MCM-41 molecular sieve with a hexagonal arrangement of mono-dimensional pores [6] has been the most widely studied. Owing to their exceptional adsorption capacities and molecular sieving properties, these materials are very attractive for the design of new selective heterogeneous catalysts for the production of chemicals in a large scale, as well as for producing fine chemicals [9]. Acid and redox functions can be generated by the incorporation of heteroelements as extra-framework nanoscale oxide clusters or in their appropriate valence state as tetrahedral framework species. As the introduction of aluminum in the mesostructure is important from the point of view of acid catalysis, it is also vital to introduce transition metal elements, such as titanium, chromium and vanadium to prepare mesoporous catalysts with redox properties.

As known, the scope of partial oxidation catalysis is wide, ranging from the large-scale production of commodities to the synthesis of minute amounts of pharmaceuticals and fine chemicals. Compared with other chemical processes, the oxidation process is complex and difficult to be controlled or to be stopped at a certain stage. For these reasons, the selective catalytic oxidation is an active field of research. The driving forces for the industrial and academic research are: the formulation of alternative or new catalysts, the reduction of the number of process steps, the elimination of waste by-products and the development of new processes. Since in the industrial manufacturing of fine chemicals the selective oxidation

* Corresponding author.
E-mail address: eherrero@scdt.frc.utn.edu.ar (E.R. Herrero).

0926-860X/$ – see front matter
doi:10.1016/j.apcata.2005.10.006

transformations are still widely performed by means of large amounts of organic peroxoacids and of transition metal reagents, the use of titanosilicate-based heterogeneous catalysts may contribute remarkably to the setup of environmentally benign industrial processes. In this large context, the selective oxidation of organic compounds, and especially of the olefinic compounds, over Ti-based catalysts and H_2O_2 has gained considerable interest [10–12]. Dilute hydrogen peroxide is one of the most convenient oxidants due to its easy handling, high content of active oxygen and absence of by-products [13]. However, in the epoxidation of alkenes, several side reactions can take place, such as oxidation in allylic positions, ring-opening of the epoxide by hydrolysis or solvolysis, epoxide rearrangement or even total breakdown of the C=C double bond. Cyclohexene is one of the most difficult cases given that the first two problems, namely allylic oxidation and epoxide ring-opening, occur extensively. It is well known that with Ti-containing zeolites as catalysts and H_2O_2 in aqueous solution as the oxidant, the selective oxidation of different organic compounds can be successfully performed without the production of environmentally unfriendly side products [10,14–17]. Such microporous zeolites are widely used as commercial catalysts, but their applications are limited by their small channel diameters. Thus, the introduction of titanium in mesoporous materials such as MCM-41 results of great interest in oxidation reactions especially of bulky molecules which cannot diffuse in the pores of microporous materials [18–20]. These mesoporous materials exhibit a potential application in numerous industrial processes such as olefins epoxidation [18–21], epoxidation of unsaturated alcohols [22–24], epoxidation of vegetable oils [25], hydroxylation of aromatics [26,27], etc., but their relatively low intrinsic chemical and hydrothermal stability could hinder their practical applications [28–34]. Such mesoporous structures of MCM-41 may collapse in hot water and in aqueous solution due to silicate hydrolysis [30,35–38]. Moreover, a particular problem associated with the use of such heterogenized catalysts in the liquid phase is the possibility of leaching the active species from the framework sites of these catalysts into solution [15,39–42]. Due to these reasons, the study of the stability of Ti-MCM-41 is an important point for a successful application.

The oxidation of cyclohexene using hydrogen peroxide is frequently used as a test reaction for the catalytic evaluation of different titanium modified materials. Scheme 1 illustrates some of the typical products of cyclohexene oxidation. The cyclohexene oxide (**I**), generated by the heterolytic epoxidation of the cyclohexene double bond, and the 1,2-cyclohexanediol (**II**) side product, formed by hydrolysis of the epoxide ring, generally reflect a concerted process. In contrast, the allylic oxidation side products, 2-cyclohexen-1-one (**III**) and 2-cyclohexen-1-ol (**IV**), are often ascribed to a homolytic radical pathway [43,44]. Various authors studied the catalytic performance of Ti-MCM-41 catalysts in the oxidation reaction of cyclohexene. Sever et al. [44] reported a cyclohexene conversion near 23% with an epoxide selectivity about 11% over Ti-MCM-41 using a cyclohexene/H_2O_2 molar ratio of 4. Hagen et al. [45] informed that the cyclohexene conversion was about 10% and the epoxide selectivity was lower than 5%, being cyclohexenyl hydroperoxide and cyclohexenone the main products, on Ti-MCM-41 with H_2O_2 as oxidant. Chen et al. [46] reported that cyclohexane diol and its methyl ethers were the major products and no cyclohexene oxide was produced when they tested Ti-substituted MCM-41 mesoporous materials as catalysts for the cyclohexene oxidation with aqueous H_2O_2. Laha and Kumar [47] also reported low catalytic activity and low selectivity to cyclohexene oxide for Ti-MCM-41 in the presence of aqueous H_2O_2. Although different metal loadings in the catalyst may induce changes in the surface species and may modify, sometimes noticeably, the catalytic features [48,49], little research has been done for elucidating the effect of varying the titanium content on the catalytic activity [46]. On the other hand, although there are many reports about the synthesis and characterization of Ti-MCM-41 materials, the influence of different synthesis variables on the structural properties and the chemical environment around the Ti atoms continues even under discussion.

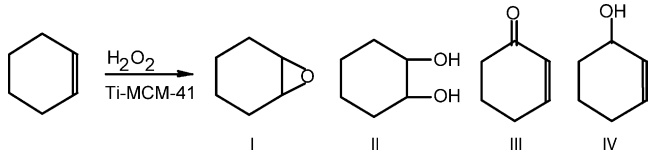

Scheme 1. Oxidation of cyclohexene with hydrogen peroxide catalyzed by Ti-MCM-41. The desired product is cyclohexene oxide (**I**), and the potential side products are 1,2-cyclohexanediol (**II**), 2-cyclohexen-1-one (**III**) and 2-cyclohexen-1-ol (**IV**).

In this work, Ti-containing MCM-41 catalysts have been prepared by direct hydrothermal synthesis and characterized by different instrumental techniques. The focus has been placed on the role of various synthesis parameters like the Ti content, the surfactant/Si ratio and the thermal process to remove the template on the physicochemical properties and the catalytic activity of these materials. The local environment of Ti(IV) centers within the mesoporous silica matrix was monitored in order to give some insight into the coordination state of the active sites, which is crucial for proper understanding of the structure and catalytic behavior of Ti-MCM-41 samples. The catalytic properties of Ti-MCM-41 were tested for the cyclohexene oxidation reaction with H_2O_2, paying special attention to the effect of metal content in the catalyst on the products distribution and the possible reaction pathways. Finally, the stability of the catalyst under the reaction conditions was also studied.

2. Experimental

The titanium-containing mesoporous materials (Ti-MCM-41) were prepared by hydrothermal synthesis using dodecyltrimethyl ammonium bromide (DTMABr) as a template. Tetraethoxysilane (TEOS) and titanium isopropoxide (TIP) were used as the Si and Ti sources, respectively. The catalysts were synthesized from gel of molar composition: Si/Ti = 10–500, TEAOH/Si = 0.30, surfactant/Si = 0.20–1.00, water/Si = 60. In a typical synthesis, TEOS (Fluka ≥98%) and TIP

(Fluka ≥98%) were vigorously mixed for 30 min. Then, 25 wt.% solution of DTMABr (Fluka ≥98%) in ethanol and 70% of the tetraethylammonium hydroxide 20 wt.% aqueous solution (TEAOH) (Fluka) were added dropwise and stirring was continued during 3 h. Finally, the remaining TEAOH and the water were further added dropwise to the milky solution which was then heated at 80 °C for 30 min to remove ethanol used in solution and produced in the hydrolysis of TEOS. The pH of the resultant gel was 11.5. This gel was transferred into Teflon-lined stainless-steel autoclave and kept in an oven at 100 °C for 7 days under autogeneous pressure. The final solid was filtered, washed and dried at 60 °C overnight (as-synthesized Ti-MCM-41). For comparison, a pure siliceous MCM-41 sample was also prepared by the same synthesis method and at the same reaction conditions. To remove the template the samples were subjected to the following treatment: Temperature programmed desorption (heating rate of 2 °C/min) with N_2 flow (5 ml/min) up to 500 °C maintaining this temperature for 6 h and further temperature programmed calcination (heating rate of 2 °C/min and air flow of 5 ml/min) up to 500 °C maintaining also this temperature for 6 h. The materials were characterized by powder X-ray diffraction (XRD), nitrogen adsorption, Fourier transformed infrared (FT-IR) and UV–vis diffuse reflectance (DRUV–vis) spectroscopy. The Ti content in the final solid products was determined by inductively coupled plasma emission spectroscopy (ICP). XRD patterns were collected in air at room temperature on a Rigaku diffractometer using Cu Kα radiation of wavelength 0.15418 nm. Diffraction data were recorded at an interval of 0.01° and a scanning speed of 2°/min was used. The interplanar distance ($d_{1\,0\,0}$) was obtained by the Bragg law using the position of the first X-ray diffraction line. The lattice parameter (a_0) of the hexagonal unit cell can be calculated by $a_0 = (2/\sqrt{3})d_{1\,0\,0}$. DRUV–vis spectra were recorded using an Optronicss OL 750-427 spectrometer in the wavelength range 200–500 nm. Specific surface area, pore size distribution and total pore volume were determined from N_2 adsorption–desorption isotherms obtained at 77 K using a Quantachrome Autosorb Automated Gas Sorption System. The surface area was determinated by the BET method and the pore size distribution was calculated by the Barrett–Joyner–Halenda (BJH) method, based on the Kelvin equation [50]. Infrared analysis of the samples was recorded on a JASCO 5300 FT-IR spectrometer either on KBr pellets or on self-supported wafers. The FT-IR spectra in the lattice vibration region were performed using KBr 0.05% wafer technique. In order to determine if the synthesized materials contain Si–OH groups, IR spectra of self-supported Ti-MCM-41 wafers (~8 mg/cm^2) were performed. Before to measure IR spectra, such samples were placed in a heating cell with CaF_2 windows connected to a vacuum line and evacuated for 8 h at 400 °C.

The cyclohexene oxidation reactions with H_2O_2 were performed at 70 °C under vigorous stirring in 2 ml glass vials placed in a temperature controlled water bath. Typically, the reaction mixture for each vial consisted of 91.90 mg of cyclohexene (Baker ≥98%), 26.60 mg of hydrogen peroxide (35 wt.%, Riedel-de Haen), 678.30 mg of acetonitrile (Cicarelli) and 9.00 mg of catalyst. In all cases, the oxidant to substrate molar ratio was 1:4 in order to minimize the possible Ti leaching [20]. The vials were withdrawn at different sampling times and analyzed by gas chromatography (Hewlett Packard 5890 Series II) using a capillary column (cross-linked methyl-silicone gum, 30 m long) and flame ionization detector. Additionally, the GC–MS (Shimadzu-QP 5050 A) analyses were performed in order to identify the reaction products. The total conversion of H_2O_2 was measured by iodometric titration. The cyclohexene conversion was defined as: cyclohexene conversion × 100/theoretically possible conversion (% of max.) [20,51]. The yields were calculated as: cyclohexene conversion (% of max.) × selectivity to reaction products/100. The turnover number (TON) was defined as moles of cyclohexene converted/mole of Ti. To take into account possible deactivation and/or by-product formation, which frequently appear after long reaction times and affect the productivity unfavorably, the performance data were compared at the end of the catalytic run. Catalyst stability was tested by separating the used catalyst from the reaction solution. It was calcined in air at 500 °C overnight before it was reused in other catalytic cycle.

3. Results and discussion

3.1. Influence of surfactant/Si ratio

Table 1 summarizes the physical properties of calcined Ti-MCM-41 samples prepared at a Si/Ti molar ratio of 20 and with different surfactant/Si molar ratios in the synthesis gel. The XRD patterns of the samples are shown in Fig. 1. All samples exhibit a main reflection peak corresponding to the (1 0 0) plane at a low angle (around 2θ = 2–3°). The other peaks have lower intensities and occur below 2θ = 10°; no diffractions were seen at higher angles [52]. The main peak becomes more intense and narrower, indicating more degree of order, for samples prepared with surfactant/Si ratio of approximately 0.30–0.40. The relatively

Table 1
Textural properties of Ti-MCM-41 samples (Si/Ti = 20) with different surfactant/Si ratios in the synthesis gel

Sample number	Surfactant/Si (molar ratio)	2θ (1 0 0) (°)	$d_{1\,0\,0}$ (nm)	a_0 (nm)	Surface area (m^2/g)
1	0.20	2.577	3.428	3.959	1336
2	0.30	2.627	3.363	3.883	1400
3	0.40	2.651	3.333	3.848	1447
4	0.60	2.571	3.436	3.968	1022
5	1.00	2.554	3.459	3.994	1158

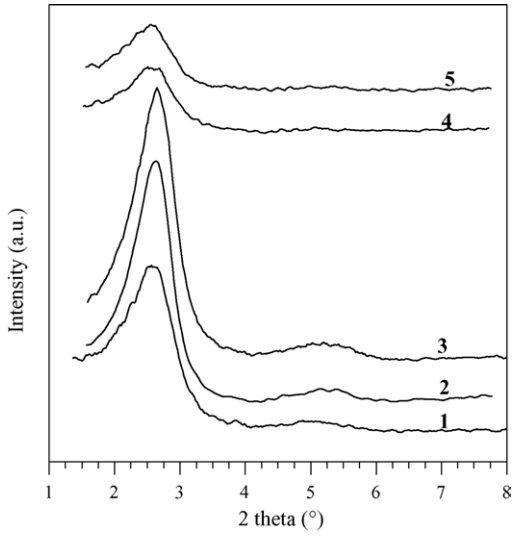

Fig. 1. XRD patterns of Ti-MCM-41 samples (Si/Ti = 20) with different surfactant/Si molar ratios. The numbers in the figure correspond to the sample numbers in Table 1: surfactant/Si = 0.20 (**1**), 0.30 (**2**), 0.40 (**3**), 0.60 (**4**), 1.00 (**5**).

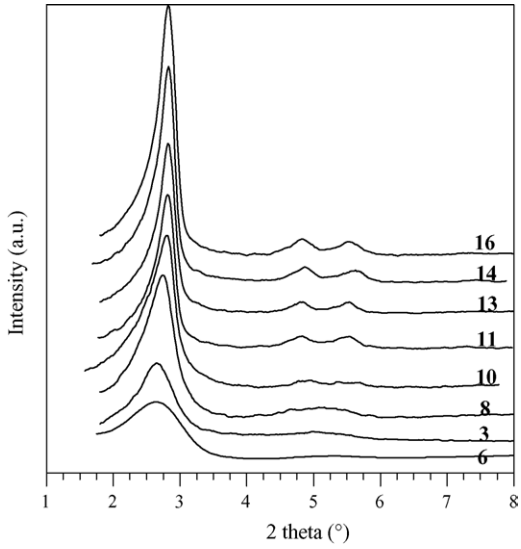

Fig. 2. XRD patterns of Ti-free (Sample **16**) and Ti-containing MCM-41 samples (surfactant/Si = 0.40). The numbers in the figure correspond to the sample numbers in Table 2: Si/Ti = 10 (**6**), 20 (**3**), 40 (**8**), 60 (**10**), 90 (**11**), 160 (**13**), 234 (**14**).

well-defined materials could not be obtained when the surfactant/Si ratio was greater than 0.50. Such difference in structure is also reflected to some extent on the values of their specific surface areas listed in Table 1. The interplanar distance ($d_{1\,0\,0}$) and the hexagonal unit cell parameter (a_0) of the samples, estimated by XRD, are presented in Table 1. The $d_{1\,0\,0}$ values were reported to be very sensitive to the degree of organization of the product [53]. As it can be observed in our data, the (1 0 0) reflections moved slightly to lower angle and concurrently $d_{1\,0\,0}$ spacing and lattice parameter (a_0) increased when long-range order of MCM-41 diminished. Therefore, it demonstrates that the surfactant/Si ratio can influence the packing of the surfactant and consequently the long-order structure to a certain degree.

3.2. Influence of titanium content

Table 2 summarizes the textural properties and chemical composition of the Ti-MCM-41 samples prepared at a surfactant/Si molar ratio of 0.40 and with different Si/Ti molar ratios in the synthesis gel. Although the incorporation of Ti decreases the specific surface area to some extent compared with pure silica MCM-41 (BET surface area of 2040 m^2/g), almost all catalysts prepared in this study possess large BET surface areas above 1300 m^2/g, being typical of M41S group materials. The metal content of the samples was determined by ICP analysis as given in table.

Fig. 2 presents the XRD patterns of some of the more representative samples prepared in this work with different loadings of Ti, together with the corresponding pure silica analog. The pure siliceous material (Sample **16**) and the Ti-MCM-41 samples with the lowest Ti contents (Samples **11**, **13** and **14**) exhibit besides a sharp (1 0 0) reflection peak at approximately $2\theta = 2.82^\circ$ weak two ascribed to (1 1 0) and (2 0 0) reflections at about $2\theta = 4.8^\circ$ and 5.5°, which is characteristic of a highly ordered structure of a hexagonal pore

Table 2
Surface properties and chemical composition of Ti-MCM-41 with different Ti contents and corresponding pure silica MCM-41 (surfactant/Si ratio = 0.40)

Sample number	Si/Ti[a] (molar ratio)	Ti content[b] (wt.%)	2θ (1 0 0) (°)	$d_{1\,0\,0}$ (nm)	a_0 (nm)	Surface area (m^2/g)
6	10	3.22	2.646	3.339	3.855	1357
3	20	2.50	2.651	3.333	3.848	1447
7	30	2.00	2.677	3.300	3.811	1490
8	40	1.54	2.741	3.223	3.722	1541
9	50	1.21	2.741	3.223	3.722	1545
10	60	1.12	2.812	3.142	3.628	1546
11	90	0.75	2.815	3.138	3.624	1580
12	120	0.59	2.823	3.130	3.614	1620
13	160	0.50	2.823	3.130	3.614	1654
14	234	0.24	2.825	3.127	3.611	1738
15	500	0.10	2.827	3.125	3.609	1995
16	∞	0.00	2.827	3.125	3.609	2040

[a] In synthesis gel.
[b] In final solid product.

array [1,2,54]. As the content of Ti is increased, the main XRD peak slightly shifts towards a lower diffraction angle consistent with a probable incorporation of Ti into the MCM-41 structure [55]. In addition, there is a decrease in the intensity of this first peak besides an evident broadening for all peaks with increasing amounts of Ti, which could be due to a reduction in the long-range order of the structure as well as to the formation of smaller particle domains after the incorporation of metal cation [56,57]. So, a Si/Ti ratio lower than 60 in the synthesis gel (corresponding to a Ti content higher than 1.12 wt.%) would not be beneficial to the formation of the long-range ordered structures indicating that the Ti ions in the gel change in some way the good organization of the silicate species with the surfactant molecules. No diffraction peaks in the region of higher angles (10–50°) could be observed indicating the absence of bulk anatase in the samples and suggesting that Ti-MCM-41 sample is a pure phase [58].

Nitrogen adsorption–desorption isotherms along with the corresponding BJH pore size distribution (inset) for Samples **3** (Si/Ti = 20) and **11** (Si/Ti = 90), which can be taken as representative of the other samples, are shown in Fig. 3. Both samples exhibit type IV isotherms with a sharp inflection at a relative pressure around $P/P_0 = 0.15–0.25$ and a corresponding narrow and strong band in the pore size distribution curve, which is characteristic of well ordered mesoporous materials with a narrow and uniform pore size distribution [47,59]. The inflection in the low relative pressure range becomes sharper for the sample with the lower Ti loading (Sample **11**) indicating a narrower pore size distribution and a higher structural order according to the XRD results. However, these isotherms also show small hysteresis loops in both the lower and higher pressure regions. According to literatures [60,61], such loops could be caused by particle–particle porosity, significant larger pores as well as by some mesopore disorder in shape. The total pore volume of the samples was calculated from the isotherm by the adsorption at $P/P_0 = 0.95$ [62] and the pore size distribution has been determined on the basis of BJH analysis [50]. The pore volume and the pore diameter for Sample **11** (0.75 wt.% of Ti) are 1.25 cm^3/g and 21.20 Å, respectively, but it decreases to 1.05 cm^3/g and 19.90 Å, respectively, for Sample **3** (2.50 wt.% of Ti). From the difference between the pore diameter and a_0 parameter obtained by XRD (Table 2), it is possible to estimate that the wall thickness is about 19 Å for Sample **3** and 15 Å for Sample **11**, similar to the values informed for Ti-MCM-41 [23,63,64]. Moreover, these results would agree with the thicker walls already reported for Ti-containing MCM-41 with respect to Ti-free MCM-41 [23,63,64].

DRUV–vis spectroscopy is a very sensitive method for characterization of the coordination environment of Ti in zeolite framework [65,66]. The DRUV–vis spectra of some of the more representative Ti-MCM-41 samples prepared at a surfactant/Si molar ratio of 0.40 and with different Ti contents are shown in Fig. 4. The intense ligand-to-metal charge transfer band at 210 nm present in all our samples clearly indicates that most of Ti ions are isolated and in tetrahedral (T_d) coordination [56,57,67,68]. A shoulder at 250–270 nm becomes significant in the samples with relatively high Ti content indicating the

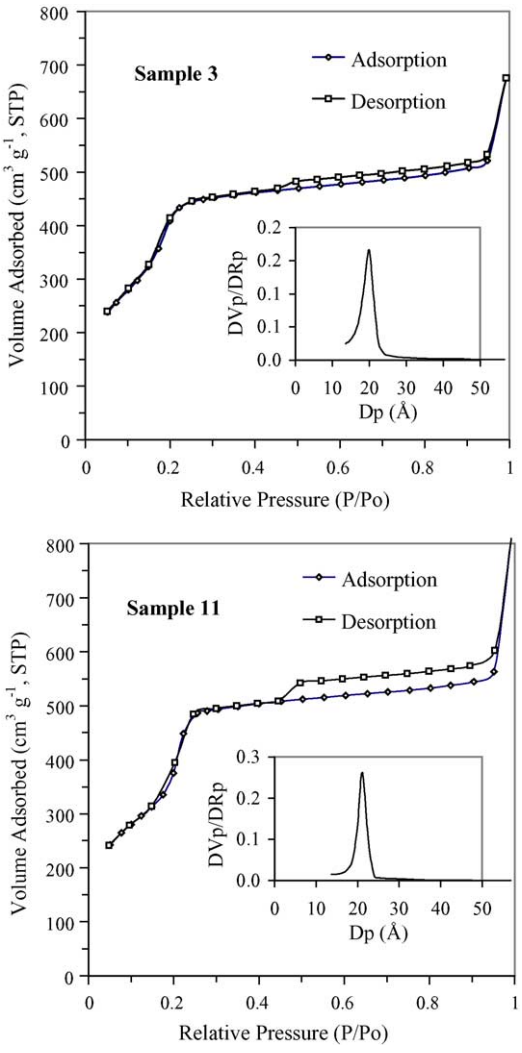

Fig. 3. Nitrogen adsorption–desorption isotherm and pore size distribution (inset) of Samples **3** (Si/Ti = 20) and **11** (Si/Ti = 90). The pore size distribution is calculated by plotting the derivative of the pore volume and the pore radius (DV_p/DR_p) against the D_p.

presence of higher coordinated Ti species (in penta- or octahedral coordination) co-existing to a small extent with the tetrahedral Ti sites. This higher coordination environment of Ti could appear upon hydration by insertion of water molecules as extraligands to the Ti T_d species during preparation [56,67–70]. Both the highly hydrophilic surface and the high surface area of these materials yield a high water adsorption capacity which would lead to a high hydration of surface Ti ions. The possibility of some Ti–O–Ti clustering in the framework due to an incipient oligomerization of Ti species containing Ti–O–Ti bonds cannot be unequivocally excluded [68,71,72]. On the other hand, compared to the bulk anatase TiO_2, the lack of an absorption band characteristic of octahedral extra-framework titanium at about 300–330 nm in all the samples suggests that no separated titania (anatase) phase is formed during the synthesis process [20]. Therefore all the catalysts synthesized by us with Ti contents in the 0.10–3.22 wt.% range present most of the Ti occupying a site-isolated position in the framework [56,57,67,73]. Moreover, in contrast with other results [57], the

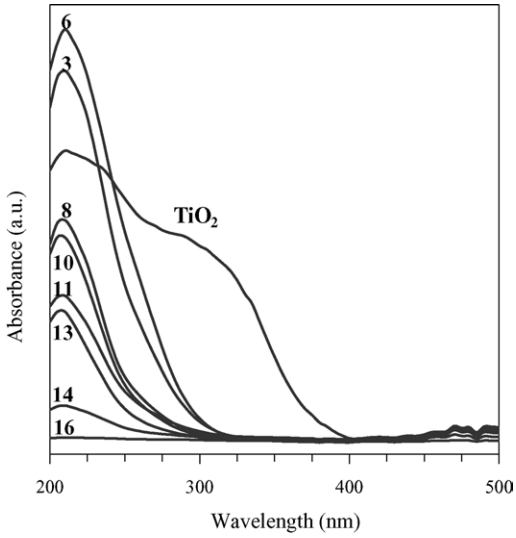

Fig. 4. DRUV–vis spectra of Ti-free (Sample **16**) and Ti-containing MCM-41 samples (surfactant/Si = 0.40). The numbers in the figure correspond to the sample numbers in Table 2: Si/Ti = 10 (**6**), 20 (**3**), 40 (**8**), 60 (**10**), 90 (**11**), 160 (**13**), 234 (**14**).

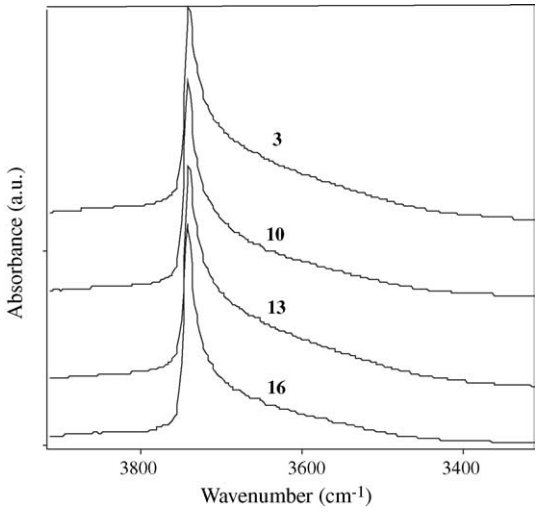

Fig. 6. FT-IR spectra in the 3300–3900 cm^{-1} range of Ti-free (Sample **16**) and Ti-containing MCM-41 samples (surfactant/Si = 0.40). The numbers in the figure correspond to the sample numbers in Table 2: Si/Ti = 20 (**3**), 60 (**10**), 160 (**13**).

intensity of the 210 nm band is substantially increased and the position of the maximum does not shift towards higher wavelengths with increasing Ti content. Such a behavior suggests that the tetrahedral component of Ti(IV) is prevalent even in the samples synthesized with high Ti content. It can be also remarked that Sample **6**, despite having a less-defined XRD pattern, still shows the Ti in framework positions and no extra-framework Ti species are detected. The DRUV–vis spectrum of pure siliceous MCM-41 does not contain any bands and it is given only for comparison with the Ti-MCM-41.

The infrared spectra in the 400–1400 cm^{-1} range for KBr-pelletized siliceous MCM-41 and Ti-MCM-41 samples are shown in Fig. 5. Two bands at around 1082 and 1228 cm^{-1} associated to internal and external asymmetric Si–O stretching modes as well as two bands (800 and 457 cm^{-1}) assigned to symmetric stretching and tetrahedral bending of Si–O bonds, respectively, can be observed. A strong band at 962 cm^{-1} is clearly visible in the FT-IR spectra of Ti-MCM-41 samples. For Ti-containing zeolites, the band at 962 cm^{-1} is believed to be a consequence of the stretching vibration of SiO units bound to Ti atoms [74–76]. However, caution is required in assigning this band since pure silica MCM-41 also exhibits such a band around 962 cm^{-1} attributed to the ν(SiOH) vibration of silanol groups at the defect sites present in the mesoporous structure. Thus, this band can be interpreted in terms of the overlapping of both Si–OH groups and Ti–O–Si bonds vibrations [77]. Although some authors [78] consider that a Ti content of approximately 1.50 wt.% in the Ti-MCM-41 catalysts is too small to cause any changes of the FT-IR spectra, we have observed that the integrated area of 962 cm^{-1} band with respect to the integrated area of ν_{sy}(Si–O–Si) band increases according to the amount of Ti incorporated in the catalyst even when the Ti content is as small as 0.10 wt.%. On the other hand, in order to inspect the OH region for the MCM-41 materials, Fig. 6 shows the spectra of some of the more representative samples synthesized in this study in the 3300–3900 cm^{-1} range. An intense band at 3740 cm^{-1} is observed in all our catalysts due to the SiOH groups sitting inside on the wall and outside as terminal OH groups. Its intensity remains unchanged with growing Ti content which could indicate that the amount of silanol groups would not be modified by the incorporation of Ti in the material. Taking into account the above results, we can suggest that a systematic increase of the IR absorption band at 962 cm^{-1} with the increase of Ti content can be taken as a reasonable proof of the Ti(IV) incorporating into the framework of MCM-41. In addition, when the integrated area ratio of the 962/800 cm^{-1} IR bands is plotted against the framework Ti content (Fig. 7), a linear relationship was established. This

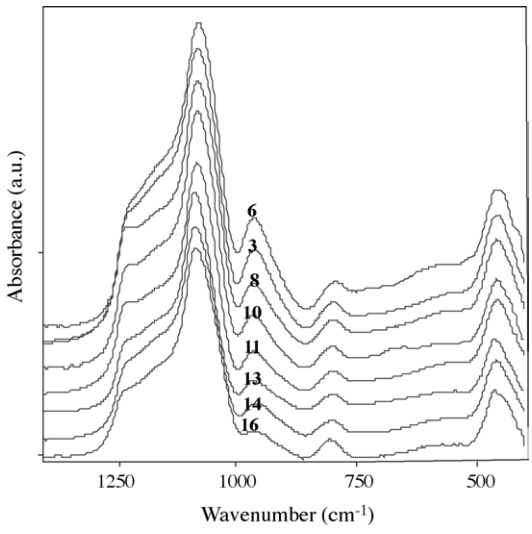

Fig. 5. FT-IR spectra in the 400–1400 cm^{-1} range of Ti-free (Sample **16**) and Ti-containing MCM-41 samples (surfactant/Si = 0.40). The numbers in the figure correspond to the sample numbers in Table 2: Si/Ti = 10 (**6**), 20 (**3**), 40 (**8**), 60 (**10**), 90 (**11**), 160 (**13**), 234 (**14**).

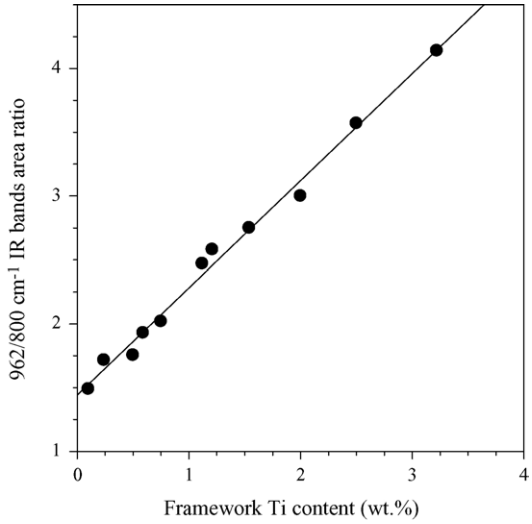

Fig. 7. Integrated area ratio of the 962/800 cm^{-1} IR bands vs. the framework titanium content.

linear dependence of such areas ratio on framework Ti loading seems to indicate that an IR study could allow us a preliminary prediction of the amount of Ti(IV) incorporated into the framework of MCM-41.

3.3. Influence of post-synthesis treatment

Fig. 8 shows the XRD patterns for Sample **8** (surfactant/Si ratio = 0.40 and Si/Ti ratio = 40), ''as-synthesized'' and after post-synthesis thermal treatment for template removal. As it can be seen, the (1 0 0) Bragg reflection increases sharply in intensity upon removal of the DTMABr ion template in contrast with the results reported by other authors who observed a reduction of the structural organization during calcination [78]. In accordance with earlier reports [44,78,79] the thermal treatment of the sample produced a small (<10%) contraction of the unit cell (a_0 changed from 4.030 to 3.722 nm) attributed

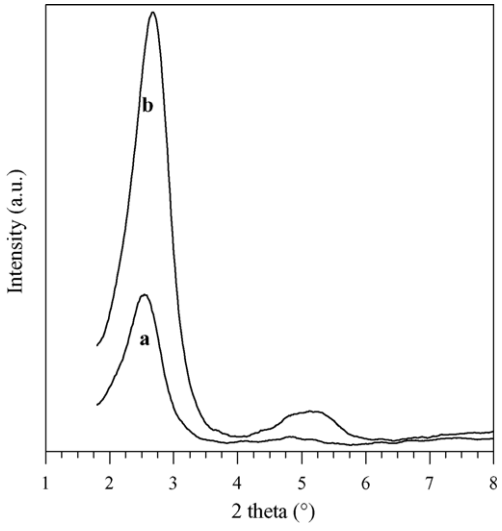

Fig. 8. XRD patterns of the Sample **8** (surfactant/Si ratio = 0.40 and Si/Ti ratio = 40): (a) as-synthesized and (b) after post-synthesis thermal treatment.

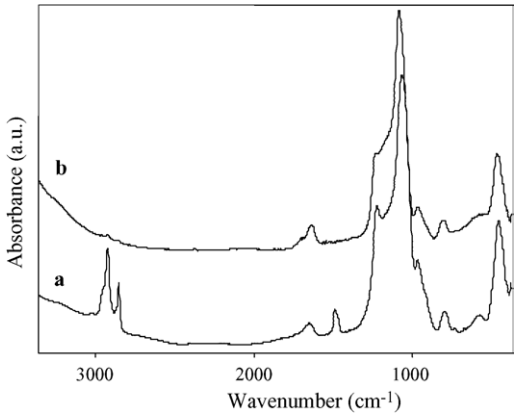

Fig. 9. FT-IR spectra in the 400–3400 cm^{-1} range of the Sample **8** (surfactant/Si ratio = 0.40 and Si/Ti ratio = 40): (a) as-synthesized and (b) after post-synthesis thermal treatment.

to the loss of the occluded organic surfactant located within the pores as well as to a further condensation of the silica lattice during the high temperature treatment. It is important to make clear that all samples synthesized in this study showed the same feature upon post-synthesis thermal treatment. On the other hand, the template removal method employed in this work, using temperature programmed desorption under N_2 flow and subsequent temperature programmed calcination under air flow, has been previously reported to produce the minor lattice contractions and long-range ordered structures in materials type MCM-41 [80].

In addition, the DRUV–vis spectra of both as-synthesized and calcined samples (not shown here) exhibit a band at 210 nm of similar intensity. Thus, in opposition to other authors [78] who observed that some of the Ti atoms left the tetrahedral MCM-41 framework after calcination, the template removal method employed by us did not cause substantial modifications in the coordination environment of Ti.

Fig. 9 shows the IR spectra of Sample **8** ''as-synthesized'' and after post-synthesis thermal treatment in the region of 400–3400 cm^{-1}. As it can be seen, the as-synthesized sample exhibits absorption bands around 2924, 2854 and 1489 cm^{-1} corresponding to asymmetric and symmetric C–H stretching and C–H bending vibrations of the surfactant molecules. Such bands disappear for the calcined sample indicating the total removal of organics upon calcination. Moreover, absorption bands at 1620–1650 cm^{-1} are caused by deformational vibrations of adsorbed water molecules [81]. On the other hand, the absorption bands corresponding to the framework vibrations region are slightly shifted toward higher frequencies in the calcined sample. This fact would reflect the formation of new Si–O–Si and Si–O–Ti bridges due to an increased network cross-linking [79,80,82] and consequently it would be accounting for the lattice contraction and structural stabilization of Ti-MCM-41 during the post-synthesis thermal treatment. Furthermore, the intensity of 962 cm^{-1} band assigned to both asymmetric Si–O–Ti bonds and silanol groups in the framework, is slightly increased after calcination. Such a feature may be taken as further evidence of that the titanium remains part of the framework after the post-synthesis

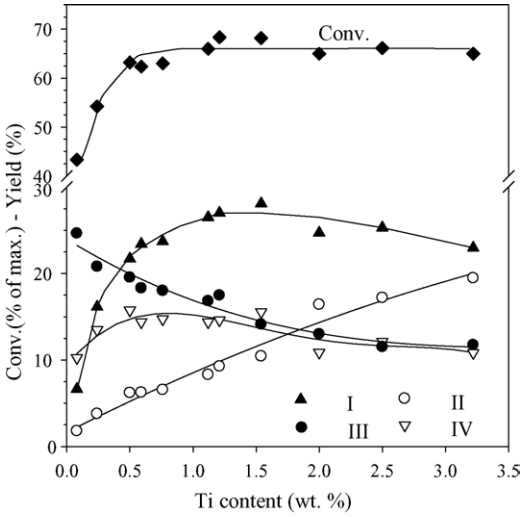

Fig. 10. Influence of Ti content in Ti-MCM-41 on the cyclohexene oxidation using H_2O_2 as oxidant. Reaction conditions: cyclohexene/H_2O_2 (mol/mol) = 4; catalyst = 9.80% of the substrate; temperature: 70 °C; reaction time: 7 h.

treatment apart from corroborating the mentioned increased network cross-linking.

3.4. Catalytic evaluation

The influence of the amount of Ti incorporated in the MCM-41 framework on cyclohexene conversion and yield to oxidation products is shown in Fig. 10. The conversion and the epoxide yield reach maximum levels of about 67% and 28%, respectively, when Ti content is about 1 wt.%. For comparison, some other reactions were also carried out: without using any catalyst, over Ti-free MCM-41 and over amorphous TiO_2. The reaction did not proceed in the absence of the catalyst and the cyclohexene conversion on pure silica MCM-41 was very low (<4%), being the main products 2-cyclohexen-1-one (**III**) and 2-cyclohexen-1-ol (**IV**). Finally, TiO_2 showed a low activity (36%) with a very low yield to epoxide (9%). These results demonstrate that the framework Ti(IV) species are the effective active sites for the selective oxidation of cyclohexene. On the other hand, as it can be seen in Fig. 10, the catalytic activity initially increases with Ti content up to reaching the maximum conversion level and then basically keeps unchanged with growing Ti loading. Although the UV–vis spectra show that the actual number of active tetrahedral Ti sites increases proportionally with the increase in Ti loading, according to Fig. 10 this fact does not result in an increase of activity above a 1 wt.% Ti loading. This suggests that many of the Ti sites are deactivated and are not effectively used for the higher loadings at the reaction time studied. As it is evidenced by the broadening of the main UV–vis band, the presence of higher coordinated Ti species at higher Ti contents is consistent with water molecules adsorbed on the catalyst. These molecules may react with the formed epoxide via epoxide ring-opening reactions leading to the formation of 1,2-cyclohexanediol (**II**) as side product, which could be favored by increasing acid Ti sites. Such diols can block the Ti active centers, as it is discussed below, reducing their availability. In fact, epoxide yield increases up to 28% at 1 wt.% Ti content and then decreases steadily with the increase in Ti content, while the amount of diol increases. On the other hand, the allylic oxidation side reactions occur to a small extent being unfavored by increasing Ti content in the MCM-41 structure. At low Ti contents, the yield to 2-cyclohexen-1-ol (**IV**) increases concurrently as the epoxide yield increases. This finding suggests that the alcohol could also arise from a secondary rearrangement of the epoxide. It is very important to note that the epoxide is our main reaction product on Ti-MCM-41 along the range of Ti contents studied. By contrast with other results [44–47] that show a low catalytic performance of Ti-MCM-41 catalysts in the cyclohexene epoxidation with H_2O_2 (conversions about 10–20% and epoxide yields lower 10%), our catalysts exhibit very good activity achieving a maximum cyclohexene conversion of 67% with a high yield to epoxide (about 28%), under similar reaction conditions.

The active catalytic species in the oxidation reactions with H_2O_2 over Ti-containing zeolites is a complex containing a hydroperoxo ligand [83]. The nucleophilic attack of the double bond of the alkene on an oxygen atom of such a complex leads to the epoxide formation. The reactivity of the Ti hydroperoxy sites depends on the geometry of the silica environment which affects the electron density of the active oxygen. On the other hand, too strong acidic centers are unfavorable for the epoxidation. Thus, taking this statement into account, the excellent performance of the Ti-MCM-41 catalysts synthesized by us in the epoxidation of cyclohexene may result from its structural properties and/or an appropriate chemical surrounding around the Ti atoms.

Fig. 11 shows the ratio of the (**I** + **II**)/(**III** + **IV**) products yields and the ratio of the **I/II** product yield at different Ti contents. Initially, the first ratio strongly increases indicating that the heterolytic epoxidation pathway would be favored with respect to the homolytic allylic oxidation pathway with increasing Ti loading. Nevertheless, such a ratio only slightly increases as Ti content is increased beyond the 1.5 wt.% level. Comparing Fig. 10 to Fig. 11, the 3.22 wt.% material is about as

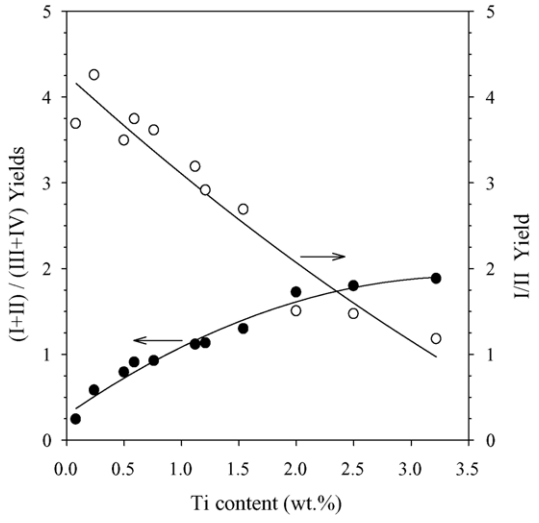

Fig. 11. Ratio of the (**I** + **II**)/(**III** + **IV**) products yields and ratio of the **I/II** product yield at different Ti contents.

Table 3
H_2O_2 selectivity and TON for the cyclohexene oxidation with H_2O_2 over Ti-MCM-41 catalysts

Ti content (wt.%)[a]	H_2O_2 selectivity (%)[b]	TON[c]
0.10	46	527
0.24	69	329
0.50	76	184
0.59	74	154
0.75	70	117
1.12	77	86
1.21	80	82
1.54	76	76
2.00	77	52
2.50	76	39
3.22	76	31

Reaction conditions: cyclohexene/H_2O_2 (mol/mol) = 4; catalyst = 9.79 wt.% of the substrate; temperature: 70 °C; reaction time: 7 h.
[a] In final solid product.
[b] H_2O_2 selectivity defined as the moles of products **I**–**IV** formed/mol of H_2O_2 reacted.
[c] TON = moles of cyclohexene converted/mol of Ti.

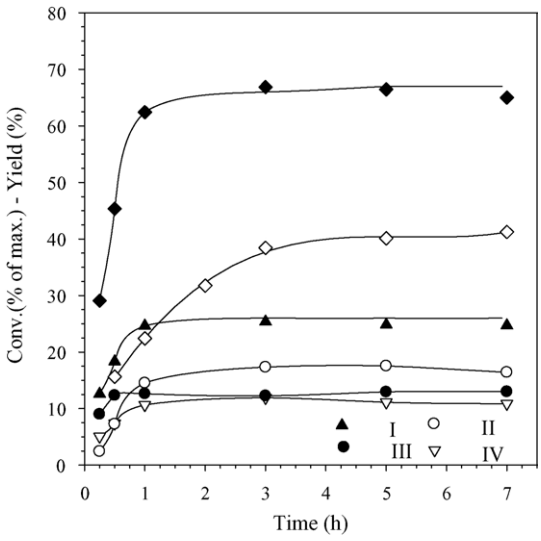

Fig. 12. Conversion of cyclohexene alone (◆), conversion of cyclohexene with addition of glycol (◇) and products yields vs. reaction time on Ti-MCM-41 (2.00 wt.% of Ti).

active as the 1.5 wt.% material but it gives a slightly higher yield of the **I + II** products (direct route). However, as the **I/II** ratio is analyzed, it can be seen that the diol is more prevalent at the higher loadings. From these results, we can conclude that a Ti content in the 1–1.5 wt.% range seems to be the optimum to achieve the highest catalytic activity with a very good epoxide yield.

On the other hand, the main side reaction for the H_2O_2 is its disproportionation to water and oxygen, which can be favored by the acid silanol groups of such mesoporous materials. Therefore, the H_2O_2 selectivity to oxidation products on pure silica MCM-41 resulted approximately 33%. However, as the metal content in MCM-41 increases, the active Ti centers would compete with the silanols by the H_2O_2 to form the hydroperoxo active complex. As it can be seen in Table 3, high H_2O_2 selectivities around 70–80% were obtained, except for the catalyst with the lowest Ti content. This feature reveals that a considerable amount of H_2O_2 could be utilized for the oxidation reaction on Ti-MCM-41 prepared by us. In addition, the turnover numbers (TON) are also given in Table 3. They decrease steadily with increasing metal content which would confirm that, as it was discussed in more detail above, much of the Ti is not effectively used during the catalytic epoxidation.

Fig. 12 illustrates the evolution of the reactants and products obtained at different reaction times using Ti-MCM-41 (2.00 wt.% of Ti). It is possible to observe a deeper insight into the catalytic activity at the beginning of the reaction. Therefore, the catalyst was active mostly in the first 2 h and then the conversion and the products yields reached a sort of asymptotic limit. Such a behavior is likely due to the adsorption of by-products onto the catalyst surface. All of the synthesized catalysts showed the same behavior with regard to the trend of the profiles of conversion and yield to products. To check the possible blocking of the active sites by adsorbed glycols, we carried out a simple experiment in which 5 wt.% of glycol was added to the reaction mixture (Fig. 12). As it can be seen, the presence of glycol in the reaction medium negatively affects the conversion. Such a feature indicates that glycol coordinates to Ti blocking many of the active centers from further reactants.

In order to evaluate the propensity to be recovered and recycled, the catalysts underwent four 7 h-catalytic cycles overall. The calcinations step before each recycle would lead to the elimination of adsorbed by-products that hinder the coordination of the reagents to the active centers. Table 4 shows conversion and products yields for each run on Ti-MCM-41 (1.12 wt.% of Ti), which is given as example. As it can be seen, the catalytic activity remained almost constant after the fourth run and the products yields did not change remarkably on passing from the first to the fourth catalytic run. These results suggest that there is not a valuable modification of the catalytic active sites during the recycling steps. In fact, as demonstrated by ICP and DRUV–vis, almost no Ti leaches out and no Ti species leave its original location even after four catalytic cycles [20]. Moreover, no structural changes occurred in the catalyst throughout the cycles since its XRD pattern was not modified. Therefore, in contrast with other authors who informed Ti leaching during the liquid phase reaction [33,46,49,84], the catalysts prepared via our optimized synthesis method exhibited good stability under the employed conditions being regenerated repeatedly without suffering loss in activity.

Table 4
Catalytic performances of the recovered Ti-MCM-41 (1.12 wt.% of Ti) in the cyclohexene oxidation with H_2O_2

Catalytic cycles	Conversion (% of max.)	Yields (%)			
		I	**II**	**III**	**IV**
1	66.00	26.49	8.31	14.38	16.82
2	66.10	26.30	8.80	15.00	16.00
3	67.00	24.90	8.70	15.37	18.03
4	66.50	25.58	8.50	15.48	16.94

Reaction conditions: cyclohexene/H_2O_2 (mol/mol) = 4; catalyst = 9.79 wt.% of the substrate; temperature: 70 °C; reaction time: 7 h.

4. Conclusion

Ti-MCM-41 molecular sieves with various compositions have been successfully prepared by direct synthesis and compared with pure siliceous MCM-41. The influence of various parameters such as Ti loading, surfactant/Si ratio in the synthesis gel and thermal process to remove the template on the surface properties and the coordination environment of Ti was systematically investigated. It has been found that the optimum surfactant/Si ratio for the preparation of good crystalline materials is 0.30–0.40. MCM-41 structure allowed the incorporation of different degrees of Ti loading (between 0.10 and 3.22 wt.%) without collapsing the structure, although a lower degree of ordering was observed with the increase of metal content above 1.12%. In all cases, solids with high specific surface area, high pore volume and a narrow pore size distribution were obtained. The temperature-programmed desorption under N_2 flow and subsequent temperature programmed calcination allowed us to achieve products with better-defined structures after the surfactant removal. Ti was incorporated into the silica framework mainly in the tetrahedral isolated sites and their coordination did not change upon our template removal technique. At high Ti content, the broadening of the main UV–vis band with a shoulder at about 260–270 nm can be assigned to a higher coordination of Ti probably due to water molecules adsorbed on the catalyst as well as to the formation of some Ti–O–Ti clustering in the framework. However, a segregated TiO_2 anatase phase was not observed for any sample. In this work, the IR spectroscopy is proposed as a simple analysis technique to monitor the local environment of Ti(IV) centers within the mesoporous silica matrix. Merging the results from the DRUV–vis, FT-IR and ICP analysis, it was possible to develop a simple method for estimating the amount of Ti incorporated in mesostructure based on the fact that the relationship between the relative areas of the 962/800 cm^{-1} IR bands increases proportionally to the growing framework Ti content. The materials synthesized here showed a very good activity for the epoxidation of cyclohexene using H_2O_2 as oxidant. The cyclohexene conversion level and the nature of oxidation products were strongly influenced by the structure of the catalyst, the degree of metal loading and the chemical environment around the active sites. The main oxidation product was the cyclohexene oxide, being the by-products the corresponding glycol and allylic oxidation products. The epoxide yield reached a maximum value of 28% (conversion = 67%) at an optimum metal content in the catalyst of approximately 1 wt.%. The presence of glycol adsorbed on Ti centers is the most probable reason for which many of the Ti sites are inactive for the higher loadings. Finally, the catalysts could be recycled after regeneration without suffering activity loss.

Acknowledgements

This work was supported by the CONICET, the A.C.C. and the UTN-FRC of Argentina. The authors thank Dr. M. Baltanás (INTEC, Santa Fe, Argentina) for help in recording DRUV–vis data and Dr. Alfredo Aguilar (CIMAV, Chihuahua, México) for help in recording nitrogen adsorption data.

References

[1] T. Yanagiswa, T. Shimizu, K. Kuroda, C. Kato, Bull. Chem. Soc. Jpn. 63 (1990) 988.
[2] J. Beck, C. Chu, I. Johnson, C. Kresge, M. Leonowicz, W. Roth, J. Vartuli, WO 91/11390 (1991).
[3] C. Kresge, M. Leonowicz, W. Roth, J. Vartuli, J. Beck, Nature 359 (1992) 710.
[4] J. Beck, J. Vartuli, W. Roth, M. Leonowicz, C. Kresge, K. Schmidt, C. Chu, D. Olson, E. Sheppard, S. McCullen, J. Higgins, J. Schenkler, J. Am. Chem. Soc. 114 (1992) 10834.
[5] S. Inagaki, Y. Fukushima, K. Kuroda, J. Chem. Soc., Chem. Commun. (1993) 680.
[6] J. Vartuli, K. Schmidt, C. Kresge, W. Roth, M. Leonowicz, S. McCullen, S. Hellring, J. Beck, J. Schlenker, D. Olson, E. Sheppard, Chem. Mater. 6 (1994) 2317.
[7] P. Tanev, T. Pinnavaia, Science 271 (1995) 1267.
[8] S. Bagshaw, E. Prouzet, T. Pinnavaia, Science 269 (1995) 1242.
[9] P. Venuto, Stud. Surf. Sci. Catal. 105 (1997) 811.
[10] I. Arends, R. Sheldon, M. Wallau, U. Schuchardt, Angew. Chem. Int. Ed. Eng. 36 (1997) 1144.
[11] B. Notari, Adv. Catal. 41 (1996) 253.
[12] J. van der Waal, M. Rigutto, H. Van Bekkum, Appl. Catal. A 167 (1998) 331.
[13] W. Sanderson, Pure Appl. Chem. 72 (2000) 1289.
[14] M. Clerici, P. Ingallina, J. Catal. 140 (1993) 71.
[15] R. Sheldon, M. Wallau, I. Arends, U. Schuchardt, Acc. Chem. Res. 31 (1998) 485.
[16] A. Corma, P. Esteve, A. Martinez, S. Valencia, J. Catal. 152 (1995) 18.
[17] N. Jappar, Q. Xia, T. Tatsumi, J. Catal. 180 (1998) 132.
[18] A. Corma, M. Navarro, J. Perez-Pariente, J. Chem. Soc., Chem. Commun. (1994) 147.
[19] A. Corma, M. Navarro, J. Perez-Pariente, F. Sanchez, Stud. Surf. Sci. Catal. 84 (1994) 69.
[20] M. Cagnoli, S. Casuscelli, A. Alvarez, J. Bengoa, N. Gallegos, N. Samaniego, M. Crivello, G. Ghione, C. Perez, E. Herrero, S. Marchetti, Appl. Catal. A: Gen. 287 (2) (2005) 227.
[21] G. Grigoropoulou, J. Clark, J. Elings, Green Chem. 5 (2003) 1.
[22] A. Wroblewska, J. Mol. Catal. A: Chem. 229 (2005) 207.
[23] C. Berlini, M. Guidotti, G. Moretti, R. Psaro, N. Ravasio, Catal. Today 60 (2000) 219.
[24] L. Davies, P. McMorn, D. Bethell, P. Bulman Page, F. King, F. Hancock, G. Hutchings, J. Catal. 198 (2001) 319.
[25] L. Rios, P. Weckes, H. Schuster, W. Hoelderich, J. Catal. 232 (2005) 19.
[26] J. He, W. Xu, D. Evans, X. Duan, C. Li, Micropor. Mesopor. Mater. 44/45 (2001) 581.
[27] K. Lin, Z. Sun, S. Lin, D. Jiang, F. Xiao, Micropor. Mesopor. Mater. 72 (2004) 193.
[28] N. Igarashi, Y. Tanaka, S. Nakata, T. Tatsumi, Chem. Lett. (1999) 1.
[29] S. Shen, S. Kawi, J. Phys. Chem. B 103 (1999) 8870.
[30] F. Di Renzo, F. Testa, J. Chen, H. Cambon, A. Galarneau, D. Plee, F. Fajula, Micropor. Mesopor. Mater. 28 (1999) 437.
[31] N. Lang, P. Delichere, A. Tuel, Micropor. Mesopor. Mater. 56 (2002) 203.
[32] V. Parvulescu, C. Anastasescu, C. Constantin, B. Su, Catal. Today 78 (2003) 477.
[33] J. Fraile, J. García, J. Mayoral, E. Vispe, Appl. Catal. A: Gen. 245 (2003) 363.
[34] F. Xiao, Catal. Surv. Asia 8 (3) (2004) 151.
[35] L. Chen, S. Jaenicke, G. Chuah, Micropor. Mater. 12 (1997) 323.
[36] V. Gonzalez-Peña, I. Diaz, C. Marquez-Alvarez, E. Sastre, J. Perez-Pariente, Micropor. Mesopor. Mater. 44/45 (2001) 295.
[37] F. Diaz Mohino, J. Perez-Pariente, E. Sastre, Appl. Catal. A 205 (2001) 19.
[38] R. Mokaya, J. Chem. Soc., Chem. Commun. (2001) 933.
[39] R. Sheldon, I. Arends, H. Lempers, Catal. Today 41 (1998) 387.

[40] J. Fraile, J. García, J. Mayoral, E. Vispe, J. Catal. 189 (2000) 40.
[41] L. Davies, P. McMorn, D. Bethell, P. Bulman Page, F. King, F. Hancock, G. Hutchings, J. Mol. Catal. A: Chem. 165 (2001) 243.
[42] L. Davies, P. McMorn, D. Bethell, P. Bulman Page, F. King, F. Hancock, G. Hutchings, J. Catal. 198 (2001) 319.
[43] K. Balkus Jr., A. Khanmamedova, J. Shi, Stud. Surf. Sci. Catal. 110 (1997) 999.
[44] R. Sever, R. Alcala, J. Dumesic, T. Root, Micropor. Mesopor. Mater. 66 (2003) 53.
[45] A. Hagen, K. Schueler, F. Roessner, Micropor. Mesopor. Mater. 51 (2002) 23.
[46] L. Chen, G. Chuah, S. Jaenicke, Catal. Lett. 50 (1998) 107.
[47] S. Laha, R. Kumar, Micropor. Mesopor. Mater. 53 (2002) 163.
[48] L. Marchese, E. Gianotti, V. Dellarocca, T. Maschmeyer, F. Rey, S. Coluccia, J. Thomas, Phys. Chem. Chem. Phys. 1 (1999) 585.
[49] M. Peña, V. Dellarocca, F. Rey, A. Corma, S. Coluccia, L. Marchese, Micropor. Mesopor. Mater. 44/45 (2001) 345.
[50] E. Barrett, L. Joyner, P. Halenda, J. Am. Chem. Soc. 73 (1951) 373.
[51] S. Casuscelli, M. Crivello, C. Perez, G. Ghione, E. Herrero, L. Pizzio, P. Vázquez, C. Cáceres, M. Blanco, Appl. Catal. A: Gen. 274 (2004) 115.
[52] T. Miyaji, W. Peng, T. Tatsumi, Catal. Today 71 (2001) 169.
[53] T. Blasco, A. Corma, M. Navarro, J. Perez-Pariente, J. Catal. 156 (1995) 65.
[54] J. Beck, US Patent 5,057,296 (1991).
[55] K. Chaudhari, R. Bal, D. Srinivas, A. Chandwadkar, S. Sivasanker, Micropor. Mesopor. Mater. 50 (2001) 209.
[56] D. Trong On, S. Nguyen, V. Hulea, E. Dumitriu, S. Kaliaguine, Micropor. Mesopor. Mater. 57 (2003) 169.
[57] V. Rajakovic, S. Mintova, J. Senker, T. Bein, Mater. Sci. Eng. C 23 (2003) 817.
[58] A. Sinha, S. Seelan, T. Akita, S. Tsubota, M. Haruta, Appl. Catal. A: Gen. 240 (2003) 243.
[59] K. Murata, Y. Liu, M. Inaba, N. Mimura, Catal. Today 91/92 (2004) 39.
[60] B. Uphade, Y. Yamada, T. Akita, T. Nakamura, M. Haruta, Appl. Catal. A: Gen. 215 (2001) 137.
[61] M. Kapoor, A. Raj, Appl. Catal. A: Gen. 203 (2000) 311.
[62] S. Gregg, K. Sing, Adsorption, Surface Area and Porosity, Academic Press, 1982,, p. 113.
[63] A. Carati, G. Ferraris, M. Guidotti, G. Moretti, R. Psaro, C. Rizzo, Catal. Today 77 (2003) 315.
[64] P. Schacht, L. Noreña-Franco, J. Anchieta, S. Ramírez, I. Hernández-Pérez, L. García, Catal. Today 98 (2004) 115.
[65] S. Bordiga, S. Coluccia, C. Lamberti, L. Marchese, A. Zecchina, F. Boscherini, F. Bufa, F. Genoni, G. Leofanti, G. Petrini, G. Vlaic, J. Phys. Chem. 98 (1994) 4125.
[66] G. Ricchiarde, A. Damin, S. Bordiga, C. Lamberti, G. Spano, F. Rivetti, A. Zecchina, J. Am. Chem. Soc. 121 (2001) 11409.
[67] M. Chao, H. Lin, C. Mou, B. Cheng, C. Cheng, Catal. Today 97 (2004) 81.
[68] J. Choi, D. Kim, S. Chang, W. Ahn, Appl. Catal. A: Gen. 254 (2003) 225.
[69] L. Bonneviot, D. Trong On, A. Lopez, J. Chem. Soc., Chem. Commun. (1993) 685.
[70] C. Geobaldo, S. Bordiga, A. Zecchina, E. Giamello, Catal. Lett. 16 (1992) 109.
[71] B. Notari, Stud. Surf. Sci. Catal. 37 (1988) 413.
[72] V. Hulea, E. Dumitriu, Appl. Catal. A: Gen. 277 (2004) 99.
[73] C. Berlini, G. Ferraris, M. Guidotti, G. Moretti, R. Psaro, N. Ravasio, Micropor. Mesopor. Mater. 44/45 (2001) 595.
[74] M. Boccuti, K. Rao, A. Zecchina, G. Leofanti, G. Petrini, Stud. Surf. Sci. Catal. 48 (1989) 133.
[75] A. Thangaraj, R. Kumar, S. Mirajkar, P. Ratnasamy, J. Catal. 130 (1991) 1.
[76] K. Li, C. Lin, Catal. Today 97 (2004) 257.
[77] M. Guidotti, N. Ravasio, R. Psaro, G. Ferraris, G. Moretti, J. Catal. 214 (2003) 242.
[78] J. Gallo, I. Paulino, U. Schuchardt, Appl. Catal. A: Gen. 266 (2004) 223.
[79] G. Eimer, L. Pierella, G. Monti, O. Anunziata, Catal. Commun. 4 (2003) 118.
[80] G. Eimer, L. Pierella, G. Monti, O. Anunziata, Catal. Lett. 78 (1–4) (2002) 65.
[81] G. Oye, J. Sjoblom, M. Stocker, Micropor. Mesopor. Mater. 34 (2000) 291.
[82] M. Landau, S. Varkey, M. Herskowitz, O. Regev, S. Pevzner, T. Sen, Z. Luz, Micropor. Mesopor. Mater. 33 (1999) 149.
[83] V. Hulea, E. Dumitriu, F. Patcas, R. Ropot, P. Graffin, P. Moreau, Appl. Catal. A: Gen. 170 (1998) 169.
[84] J. Fraile, J. García, J. Mayoral, E. Vispe, J. Catal. 189 (2000) 40.